Measurement-Based FET Analytical Modeling Using the Nonlinear Function Sampling Approach

Measurement-based FET Analytical Modeling using the Nonlinear Function Sampling Approach

Teresa Martín-Guerrero, *Member, IEEE,* Alberto Santarelli, *Member, IEEE,* Gian Piero Gibiino, *Member, IEEE,* Pier Andrea Traverso, *Member, IEEE,* Carlos Camacho-Peñalosa, *Life Senior Member, IEEE,* and Fabio Filicori

***Abstract*—A novel and fast method for the measurement-based identification of an analytical FET compact model from large-signal waveforms is presented. Based on a two-tone two-port experiment, a recently published Nonlinear Function Sampling (NFS) operator providing the samples of the FET state functions in the voltage domain is here exploited, for the first time, to extract an equivalent-circuit model. The approach is demonstrated on a 250-nm GaN-on-SiC HEMT at 2.5 and 5 GHz.**

***Index Terms*—Field-effect transistors (FETs), gallium nitride (GaN), large-signal measurements, device modeling.**

I. Introduction

The design of nonlinear microwave circuits requires the availability of accurate field-effect transistor (FET) models, which should be preferably identified from experiments closely resembling the prospected device operating conditions [1]-[4]. Nevertheless, popular analytical compact models [5], [6], which provide the designer with a clear device description and are easily implemented in Computer-Aided Design (CAD) tools, are usually obtained from static or multi-bias S-parameters measurements, under operating conditions that are substantially different from the final application.

In this work, we propose a fast model extraction procedure from Continuous-Wave (CW) operation under a two-port two-tone excitation [7]. This procedure, applied to a 8×125-μm 250-nm Gallium Nitride (GaN) on Silicon Carbide (SiC) High-Electron-Mobility Transistor (HEMT), leverages on a recently published operator, referred to as *Nonlinear Function Sampling* (NFS) [8], which provides the samples of the FET state functions (conduction current and charges) in the control-voltage domain. Differently from [8], the NFS approach is here exploited to extract an analytical model, namely the Chalmers model [5], which is then validated with both CW and Third-Order Intermodulation (IM3) large-signal tests. All measurements are acquired by biasing the device for class-AB operation ($V_{GQ} = -3.4$ V, $V_{DQ} = 30$ V, $I_D \approx 80$ mA).

II. Nonlinear Function Sampling Approach

The FET in common-source configuration is driven into nonlinear operation by two single-tone power waves at independent frequencies f_A and f_B, suitably chosen to properly excite the device in an application range, yet avoiding non-quasi-static effects. Each tone is applied at gate and drain, respectively, and the incident and reflected waves are measured at the extrinsic FET ports. After parasitic de-embedding [9], the mixing products of the intrinsic voltages $\mathbf{V}_{n,m} = \{V_{GS_{n,m}}, V_{DS_{n,m}}\}^T$ and currents $\bar{\mathbf{I}}_{n,m} = \{\bar{I}_{GS_{n,m}}, \bar{I}_{DS_{n,m}}\}^T$ can be extracted at frequencies $f_{n,m} = |nf_A + mf_B|$, with $n, m = 0, \pm1, \pm2, \pm3$ ($r = |n| + |m|$ being the mixing order). In this work, this two-tone experiment was performed with a Nonlinear Vector Network Analyzer (NVNA) setup (Fig. 1a), choosing f_A = 2 GHz and f_B = 2.74 GHz to guarantee that the non-negligible mixing products (here, up to N = 10, M = 10, R = 20) do not overlap in frequency. Due to the absence of higher-order nonlinearity, f_A and f_B can be seen as incommensurate, as each acquired waveform is quasi-periodic in the physical time domain t. Yet, the two tones can be effectively treated as bi-periodic, with periods $T_A = 1/f_A$ and $T_B = 1/f_B$, by introducing an auxiliary bi-temporal domain (τ_A, τ_B) [10]. Thus, the time-domain intrinsic currents $\bar{\boldsymbol{\mathcal{I}}} = \{\bar{\mathcal{I}}_{GS}, \bar{\mathcal{I}}_{DS}\}^T$ can be represented with 2D Fourier series:

$$\begin{aligned}\bar{\boldsymbol{\mathcal{I}}}(\tau_A, \tau_B) \doteq \bar{\mathbf{I}}_{0,0} &+ \sum_{m,n} \bar{\mathbf{I}}^a_{m,n} \cos(n\omega_A\tau_A + m\omega_B\tau_B) \\ &+ \sum_{m,n} \bar{\mathbf{I}}^b_{m,n} \sin(n\omega_A\tau_A + m\omega_B\tau_B),\end{aligned} \tag{1}$$

which coincide with the waveforms in the physical time domain for $\tau_A = \tau_B = t$. Analogous expressions for the intrinsic voltages $\boldsymbol{\mathcal{V}} = \{\mathcal{V}_{GS}, \mathcal{V}_{DS}\}^T$ can be obtained in terms of $\mathbf{V}^a_{m,n}$ and $\mathbf{V}^b_{m,n}$. Assuming a quasi-static intrinsic model:

$$\bar{\mathbf{i}}(\mathbf{v}) = \mathbf{i}(\mathbf{v}) + \frac{\mathrm{d}\mathbf{q}(\mathbf{v})}{\mathrm{d}t}, \tag{2}$$

where $\bar{\mathbf{i}} = \{\bar{i}_{GS}, \bar{i}_{DS}\}^T$ and $\mathbf{v} = \{v_{GS}, v_{DS}\}^T$, $\mathbf{i}(\mathbf{v}) = \{i_{GS}(\mathbf{v}), i_{DS}(\mathbf{v})\}^T$ represents iso-dynamic I/V input and output FET conduction characteristics, while $\mathbf{q}(\mathbf{v}) = \{q_{GS}(\mathbf{v}), q_{DS}(\mathbf{v})\}^T$ includes the gate and drain quasi-static charge functions. For a given $\boldsymbol{\mathcal{V}}(\tau_A, \tau_B)$, due to the quasi-static hypothesis, it holds:

$$\bar{\boldsymbol{\mathcal{I}}}(\tau_A, \tau_B) \doteq \boldsymbol{\mathcal{I}}(\tau_A, \tau_B) + \frac{\partial \boldsymbol{\mathcal{Q}}(\tau_A, \tau_B)}{\partial \tau_A} + \frac{\partial \boldsymbol{\mathcal{Q}}(\tau_A, \tau_B)}{\partial \tau_B}, \tag{3}$$

with $\bar{\boldsymbol{\mathcal{I}}}(\tau_A, \tau_B) = \bar{\boldsymbol{i}}(\boldsymbol{\mathcal{V}}(\tau_A, \tau_B))$, $\boldsymbol{\mathcal{I}}(\tau_A, \tau_B) = \boldsymbol{i}(\boldsymbol{\mathcal{V}}(\tau_A, \tau_B))$, $\boldsymbol{\mathcal{Q}}(\tau_A, \tau_B) = \boldsymbol{q}(\boldsymbol{\mathcal{V}}(\tau_A, \tau_B))$. By expressing (3) in the frequency domain, after some algebraic manipulation, it holds:

$$\begin{aligned}\bar{\mathbf{I}}^a_{n,m} &= \mathbf{I}^a_{n,m} + 2\pi f_{n,m} \mathbf{Q}^b_{n,m} \\ \bar{\mathbf{I}}^b_{n,m} &= \mathbf{I}^b_{n,m} - 2\pi f_{n,m} \mathbf{Q}^a_{n,m}.\end{aligned} \tag{4}$$

FET state functions extraction on the basis of the known intrinsic current spectral components $\bar{\mathbf{I}}^a_{n,m}$, $\bar{\mathbf{I}}^b_{n,m}$ can be achieved in two steps: 1) the identification of the whole set of complex coefficients $\mathbf{I}^a_{n,m}$, $\mathbf{I}^b_{n,m}$, $\mathbf{Q}^a_{n,m}$, $\mathbf{Q}^b_{n,m}$ entirely defining the

T. Martín-Guerrero and C. Camacho-Peñalosa are with the Departamento de Ingeniería de Comunicaciones, Universidad de Málaga, 29010 Málaga, Spain (e-mail: teresa@ic.uma.es).

A. Santarelli, G. P. Gibiino, P. A. Traverso, and F. Filicori are with the Dept. Electrical, Electronic, and Information Engineering, University of Bologna, 40136 Bologna, Italy.

Manuscript received xx; revised xx

conduction current and charge waveforms; 2) the extraction of the conduction I/V characteristic $\mathbf{i}(\mathbf{v})$ and charge functions $\mathbf{q}(\mathbf{v})$ from their parent waveforms.

To achieve 1), the voltage domain $\mathcal{D}_v$ associated with a particular set of injected waves is partitioned into elementary cells Δv_{GS}, Δv_{DS} with central points $\tilde{\mathbf{v}}_{i,j} = \{\tilde{v}_{GS_i}, \tilde{v}_{DS_j}\}$, i, j being suitable indexes. Also, the two time-axes are discretized in $\tau_{A,l}$, $\tau_{B,k}$ points located at $\Delta\tau_A$, $\Delta\tau_B$ intervals across the periods T_A, T_B of the τ_A, τ_B axes, respectively. By reducing the discretization steps $\Delta\tau = \{\Delta\tau_A, \Delta\tau_B\}^T$, any number of samples should be obtained within any properly-dimensioned elementary cell, owing to bi-temporal interpolation. Otherwise, additional two-tone experiments with different injected tone amplitudes could be added to the dataset. Let $P_{i,j}$ be the number of samples falling into the (i,j)th elementary voltage cell for a particular choice of $\Delta\tau$. Also, let $\{\boldsymbol{\mathcal{V}}(\tau_{A,l_p}, \tau_{B,k_p})\}_{i,j}$, $p = 0, 1, \ldots, P_{i,j} - 1$, be the intrinsic voltage samples falling into the (i,j)th cell. Since the $\boldsymbol{\mathcal{I}}$ and $\boldsymbol{\mathcal{Q}}$ waveforms derive from the algebraic voltage functions $\mathbf{i}(\mathbf{v})$ and $\mathbf{q}(\mathbf{v})$, each pth sample within any voltage cell (i,j) with $P_{i,j} \geq 2$ must satisfy:

$$\begin{aligned}\mathbf{i}(\tilde{\mathbf{v}}_{i,j}) &\simeq \mathcal{I}(\tau_{A,l_p}, \tau_{B,k_p}) \simeq \frac{1}{P_{i,j}} \sum_{p=0}^{P_{i,j}-1} \mathcal{I}(\tau_{A,l_p}, \tau_{B,k_p}) \\ \mathbf{q}(\tilde{\mathbf{v}}_{i,j}) &\simeq \mathcal{Q}(\tau_{A,l_p}, \tau_{B,k_p}) \simeq \frac{1}{P_{i,j}} \sum_{p=0}^{P_{i,j}-1} \mathcal{Q}(\tau_{A,l_p}, \tau_{B,k_p}),\end{aligned} \tag{5}$$

provided that the elementary cell dimensions are small enough to justify the approximations. Relations (5), once transformed into the frequency domain and accounting for (4), lead to an over-determined system of linear equations in the unknowns $\mathbf{I}^a_{n,m}$, $\mathbf{I}^b_{n,m}$, $\mathbf{Q}^a_{n,m}$, $\mathbf{Q}^b_{n,m}$, allowing for the identification of the waveforms $\boldsymbol{\mathcal{I}}$ and $\boldsymbol{\mathcal{Q}}$.

Eventually, also 2) is performed from (5) obtaining the nonlinear model functions samples $\mathbf{i}(\tilde{\mathbf{v}}_{i,j})$, $\mathbf{q}(\tilde{\mathbf{v}}_{i,j})$ from their parent waveforms for a suitable time-domain discretization. Then, the corresponding $\mathbf{i}(\mathbf{v})$, $\mathbf{q}(\mathbf{v})$ functions can be interpolated from the retrieved samples. The expressions in (5), which result from applying the *Nonlinear Function Sampling* (NFS) operator [8], enable the FET state functions identification over the control voltage plane $\mathcal{D}_v$ from measured waveforms.

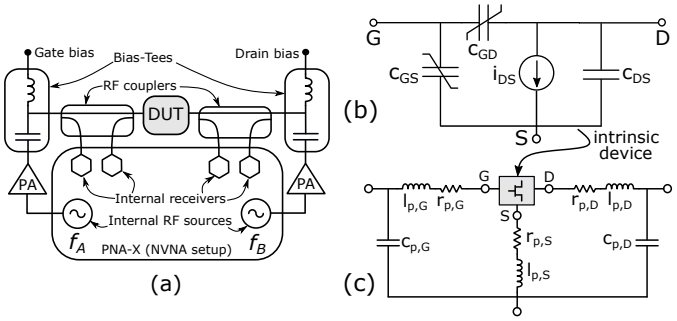

Fig. 1. (a) Block diagram of the measurement setup for the two-tone NVNA experiment. (b) Topology of the adopted equivalent-circuit model (diodes not shown). (c) Extrinsic parasitic network, whose values ($r_{p,G}$ = 1.7 Ω, $r_{p,D}$ = 1.3 Ω, $r_{p,S}$ = 0.1 Ω, $c_{p,G}$ = 30 pF, $c_{p,D}$ = 40 pF, $l_{p,G}$ = 102 pH, $l_{p,D}$ = 88 pH, $l_{p,S}$ = 12 pH) have been extracted with the method in [9].

III. Compact Model Identification and Validation

The $\mathbf{i}$ and $\mathbf{q}$ function samples obtained with the NFS approach can be used to fit a compact analytical model, which represents a well-behaved interpolator for the measured data. In the following, the extracted data are used to implement the Chalmers model [5]. Whereas the NFS-based procedure provides voltage-domain samples of the nonlinear charges $q_{GS}(\mathbf{v})$ and $q_{DS}(\mathbf{v})$, the majority of the analytical compact models, and in particular the Chalmers model, implements nonlinear capacitances $C_{GS}(v_{GS}, v_{DS})$ and $C_{GD}(v_{GS}, v_{DS})$ (see Fig. 1b) [11]. Thus, the samples of C_{GS} and C_{GD} in the voltage domain must be first obtained by differentiating $q_{GS}(\mathbf{v})$ and $q_{DS}(\mathbf{v})$, according to the following relationships:

$$\begin{aligned} C_{GS} &= \frac{\partial q_{GS}}{\partial v_{GS}} + \frac{\partial q_{GS}}{\partial v_{DS}}; \quad C_{GD} = -\frac{\partial q_{GS}}{\partial v_{DS}}; \\ C_m &= \frac{\partial q_{DS}}{\partial v_{GS}} - \frac{\partial q_{GS}}{\partial v_{DS}}; \quad C_{DS} = \frac{\partial q_{DS}}{\partial v_{DS}} + \frac{\partial q_{GS}}{\partial v_{DS}}. \end{aligned} \tag{6}$$

Then, the NFS samples for C_{GS} and C_{GD} can be used to fit the analytical parametric expressions of the Chalmers model:

$$\begin{aligned} C_{GS} &= C_{GSpi} + C_{GS0}(1 + \tanh(\phi_1))(1 + \tanh(\phi_2)); \\ C_{GD} &= C_{GDpi} + C_{GD0}(1 + \tanh(\phi_3))(1 + \tanh(\phi_4)); \end{aligned} \tag{7}$$

$$\begin{aligned} \phi_1 &= P_{10} + P_{11} v_{GS}; \quad \phi_2 = P_{20} + P_{21} v_{DS}; \\ \phi_3 &= P_{30} - P_{31} v_{DS}; \quad \phi_4 = P_{40} + P_{41} v_{GD}. \end{aligned} \tag{8}$$

Regarding the reminder part of the capacitive model, the output capacitance C_{DS} is considered bias-independent. In addition, the transcapacitance C_m is equivalently accounted for by an internal delay (τ) parameter within the i_{DS} generator expression, implementing $i_{DS}(t) = i_{DS}(v_{GS}(t-\tau), v_{DS}(t))$.

No pre-processing is needed for the NFS samples of $\mathbf{i}$. At first, a simplified five-parameters model (I_{pks}, α_s, λ, V_{pks}, P_1) for the expression of i_{DS} was considered [5], yet resulting in poor accuracy in the knee-voltage region. Eventually, a seven-parameter expression including α_r and P_2 has been adopted:

$$i_{DS} = I_{pk0} + (1 + \tanh(\psi)) \tanh(\alpha v_{DS}) (1 + \lambda v_{DS}); \tag{9}$$

$$\begin{aligned} \psi &= P_1(v_{GS} - V_{pks}) + P_2(v_{GS} - V_{pks})^2; \\ \alpha &= \alpha_r + \alpha_s(1 + \tanh(\psi)). \end{aligned} \tag{10}$$

A nonlinear least-squares method based on the trust-region algorithm[1] has been used for fitting the current and capacitance analytical expressions, resulting in the parameters in Tab. I. The fitting quality (Figs. 2 and 3a) shows that the analytical

[1]using *lsqcurvefit()* from MATLAB Curve Fitting Toolbox™ (R2019b).

TABLE I
Parameters of the Identified Chalmers Model

I_{pk0} (mA)	V_{pks} (V)	P_1 (V^{-1})	P_2 (V^{-2})	α_r (V^{-1})	α_s (V^{-1})	λ (V^{-1})
335.5	-1.037	0.3963	-0.04697	0.2577	0.2720	0.009224
C_{GSpi} (pF)	C_{GS0} (pF)	P_{10} (a.u.)	P_{11} (V^{-1})	P_{20} (a.u.)	P_{21} (V^{-1})	C_{DS} (pF)
0.7006	0.2073	1.937	0.6076	1.779	0.5303	0.4046
C_{GDpi} (pF)	C_{GD0} (pF)	P_{30} (a.u.)	P_{31} (V^{-1})	P_{40} (a.u.)	P_{41} (V^{-1})	τ (ps)
4.312e-2	0.9402	-0.8402	0.01702	3.625e-6	0.05319	5.148

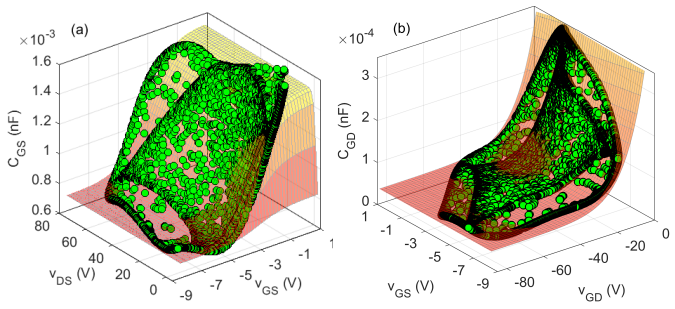

Fig. 2. Capacitance $C_{GS}(v_{GS}, v_{DS})$ (a) and capacitance $C_{GD}(v_{GS}, v_{GD})$ (b): NFS samples (green dots) and interpolation (red surface) using the parametric model in (7). Fitting deviation in terms of root mean square error (RMSE) is 9.5×10^{-5} nF and 1.5×10^{-5} nF for C_{GS} and C_{GD}, respectively.

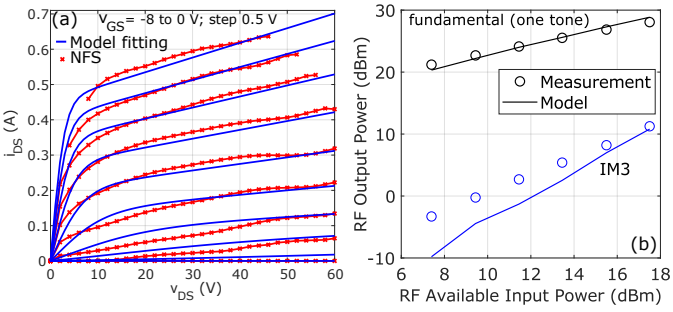

Fig. 3. (a) I/V curves: NFS samples (red) and interpolation using (9) (blue). Fitting deviation (RMSE) is 40 mA. (b) IM3 test at 2.5 GHz with $Z_L \simeq 50$ Ω and Δf =20 MHz.

models are suitable interpolators of the sampled data. In addition, by inheriting the NFS dataset properties, the obtained parametric model has been verified to be charge conservative up to the fitting accuracy.

Beyond the classic Chalmers model, GaN dispersive effects [12] are accounted for by the superposition of separate thermal and charge-trapping models. Among the possible approaches [4], [13], [14], an equivalent-voltage (v_{GS}^{eq}) above cut-off description was chosen:

$$\begin{aligned} i_{DS} &\simeq \left(1+\alpha_{\theta_m}\left(\theta-\theta^*\right)\right) i_{DS}\left(v_{GS}^{eq}, v_{DS}, \theta^*, \hat{\chi}\right); \\ v_{GS}^{eq} &\doteq v_{GS}+\alpha_{\theta_t}\left(\theta-\theta^*\right)+\alpha_{\chi}\left(\chi-\hat{\chi}\right); \end{aligned} \tag{11}$$

where θ^* and $\hat{\chi}$ are arbitrary reference values for the channel temperature (θ) and the charge-trapping state (χ), respectively. The thermal parameters α_{θ_m} =-2 mA/°C and α_{θ_t} =1.5 mV/°C, which account for the effect of temperature on electron mobility and threshold voltage, have been extracted on the basis of a thermal resistance R_θ= 14 °C/W provided by the manufacturer. The parameter $\alpha_\chi = -0.7$ V takes into account the deviation between the reference state $\hat{\chi}$ and the actual operating state, where the state deviations are pre-characterized with four two-tone tests as in Sec. II with different injected amplitudes, corresponding to four v_G-v_D peaks combinations. This data allows to approximate a trap-related 2D nonlinear lag function [15] in the voltage domain.

The identified analytical Chalmers model has been implemented in CAD (Keysight ADS) and tested for IM3 at 2.5 GHz (Fig. 3b) as well as for CW at 2.5 GHz and 5 GHz

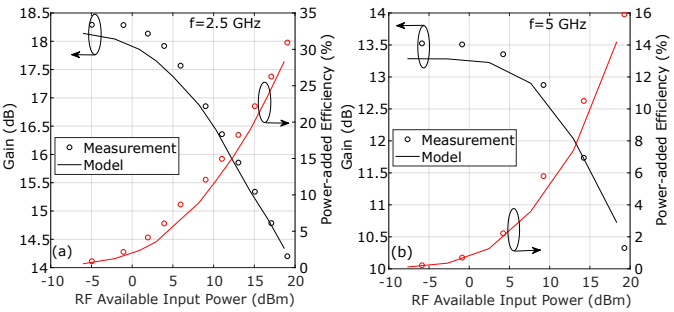

Fig. 4. Model performance prediction for a CW sweep at 2.5 GHz (a) and at 5 GHz (b).

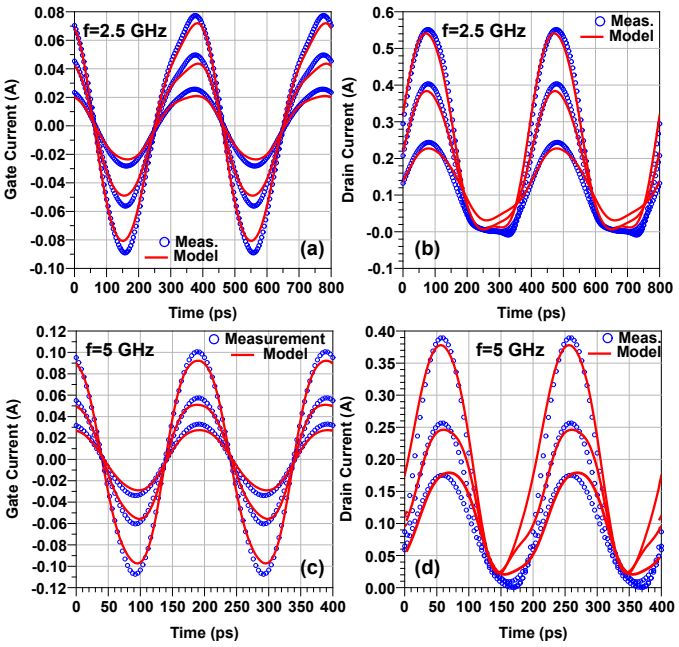

Fig. 5. Model waveform prediction under CW excitation at $f = 2.5$ GHz (a)-(b) and $f = 5$ GHz (c)-(d) with load impedance $Z_L \simeq 50$ Ω (RF available input powers 9, 15, and 19 dBm).

(Figs. 4 and 5, respectively), reporting a robust and sufficiently accurate behavior.

IV. Conclusion

In this work we described, for the first time, a direct procedure based on a recently published NFS operator for the identification of a large-signal analytical FET model, in particular the popular Chalmers model [5]. It requires an extremely reduced number of broadband acquisitions, yet allowing for arbitrarily dense samples of the conduction currents and charge functions over the whole voltage operating region. The proposed joint NFS post-processing and Chalmers analytical representation inherits native coherency between conduction and displacement current components, featuring a straightforward charge-conservative implementation. As demonstrated by the reported experimental tests under large-signal operation, good performance prediction can be achieved under realistic regimes. Compared to look-up tables [8], the extracted analytical model is easily found in CAD, and it allows for robust approximation and extrapolation of the extracted data.

REFERENCES

[1] D. Schreurs, J. Verspecht, B. Nauwelaers, A. Van de Capelle, and M. Van Rossum, "Direct Extraction of the Non-Linear Model for Two-Port Devices from Vectorial Non-Linear Network Analyzer Measurements," in *Proc. Eur. Microw. Conf.*, vol. 2, Sep. 1997, pp. 921–926.

[2] D. G. Morgan, G. D. Edwards, A. Phillips, and P. J. Tasker, "Full extraction of PHEMT state functions using time domain measurements," in *IEEE MTT-S Int. Microw. Symp. Dig.*, vol. 2, 2001, pp. 823–826.

[3] Y. Ko *et al.*, "Artificial Neural Network Model of SOS-MOSFETs Based on Dynamic Large-Signal Measurements," *IEEE Trans. Microw. Theory Techn.*, vol. 62, no. 3, pp. 491–501, March 2014.

[4] J. Xu, R. Jones, S. A. Harris, T. Nielsen, and D. E. Root, "Dynamic FET model - DynaFET - for GaN transistors from NVNA active source injection measurements," in *IEEE MTT-S Int. Microw. Symp. Dig.*, Jun. 2014, pp. 1–3.

[5] I. Angelov, H. Zirath, and N. Rosman, "A new empirical nonlinear model for HEMT and MESFET devices," *IEEE Trans. Microw. Theory Techn.*, vol. 40, no. 12, pp. 2258–2266, Dec 1992.

[6] J. C. Pedro, D. E. Root, J. Xu, and L. C. Nunes, *Nonlinear Circuit Simulation and Modeling: Fundamentals for Microwave Design*. Cambridge University Press, 2018.

[7] D. Niessen, G. P. Gibiino, R. Cignani, A. Santarelli, D. Schreurs, and F. Filicori, "Charge-Controlled GaN FET Modeling by Displacement Current Integration From Frequency-Domain NVNA Measurements," *IEEE Trans. Microw. Theory Techn.*, vol. 64, no. 12, pp. 4382–4393, Dec 2016.

[8] T. M. Martín-Guerrero, A. Santarelli, G. P. Gibiino, P. A. Traverso, C. Camacho-Peñalosa, and F. Filicori, "Automatic extraction of measurement-based large-signal FET models by nonlinear function sampling," *IEEE Trans. Microw. Theory Techn.*, vol. 68, no. 5, pp. 1627–1636, 2020.

[9] G. P. Gibiino, A. Santarelli, R. Cignani, P. A. Traverso, and F. Filicori, "Measurement-Based Automatic Extraction of FET Parasitic Network by Linear Regression," *IEEE Microw. Wireless Compon. Lett.*, vol. 29, no. 9, pp. 598–600, Sep. 2019.

[10] F. Filicori and V. A. Monaco, "Computer-aided design of non-linear microwave circuits," *Alta Frequenza*, vol. 57, no. 7, pp. 355–378, 1988.

[11] P. Aaen, J. A. Plá, and J. Wood, *Modeling and characterization of RF and microwave power FETs*. Cambridge University Press, 2007.

[12] S. C. Binari, K. Ikossi, J. A. Roussos, W. Kruppa, Doewon Park, H. B. Dietrich, D. D. Koleske, A. E. Wickenden, and R. L. Henry, "Trapping effects and microwave power performance in algan/gan hemts," *IEEE Trans. Electron Devices*, vol. 48, no. 3, pp. 465–471, 2001.

[13] L. C. Nunes, J. M. Gomes, P. M. Cabral, and J. C. Pedro, "A new nonlinear model extraction methodology for GaN HEMTs subject to trapping effects," in *IEEE MTT-S Int. Microw. Symp. Dig.*, 2015, pp. 1–4.

[14] G. P. Gibiino, A. Santarelli, and F. Filicori, "A GaN HEMT global large-signal model including charge trapping for multibias operation," *IEEE Trans. Microw. Theory Techn.*, vol. 66, no. 11, pp. 4684–4697, 2018.

[15] A. Santarelli, R. Cignani, D. Niessen, G. P. Gibiino, P. A. Traverso, D. Schreurs, and F. Filicori, "Multi-bias nonlinear characterization of gan fet trapping effects through a multiple pulse time domain network analyzer," in *2015 10th European Microwave Integrated Circuits Conference (EuMIC)*. IEEE, 2015, pp. 81–84.